JOURNAL OF GEOPHYSICAL RESEARCH: SOLID EARTH, VOL. 118, 1–14, doi:10.1002/jgrb.50189, 2013

Systematic relocation of seismicity on Hawaii Island from 1992 to 2009 using waveform cross correlation and cluster analysis

Robin S. Matoza,[1] Peter M. Shearer,[1] Guoqing Lin,[2] Cecily J. Wolfe,[3,4] and Paul G. Okubo[5]

Received 28 November 2012; revised 8 April 2013; accepted 10 April 2013.

[1] The analysis and interpretation of seismicity from mantle depths to the surface play a key role in understanding how Hawaiian volcanoes work. We present results from a comprehensive and systematic re-analysis of waveforms from 130,902 seismic events recorded by the U.S. Geological Survey Hawaiian Volcano Observatory permanent seismic network from January 1992 to March 2009. We compute high-precision relative relocations for 101,390 events (77% of all events considered) using waveform cross correlation and cluster analysis, resulting in a multiyear systematically processed catalog of seismicity for all of Hawaii Island. The 17 years of relocated seismicity exhibit a dramatic sharpening of earthquake clustering along faults, streaks, and magmatic features, permitting a more detailed understanding of fault geometries and volcanic and tectonic processes. Our relocation results are generally consistent with previous studies that have focused on more specific regions of Hawaii. The relocated catalog includes crustal seismicity at Kilauea and its rift zones, seismicity delineating crustal detachment faults separating volcanic pile and old oceanic crust on the flanks of Kilauea and Mauna Loa, events along inferred magma conduits, and events along inferred mantle fault zones. The relocated catalog is available for download in the supporting information.

Citation: Matoza, R. S., P. M. Shearer, G. Lin, C. J. Wolfe, and P. G. Okubo (2013), Systematic relocation of seismicity on Hawaii Island from 1992 to 2009 using waveform cross correlation and cluster analysis, *J. Geophys. Res. Solid Earth*, *118*, doi:10.1002/jgrb.50189.

1. Introduction

[2] Seismic investigations began on Hawaii Island (Figure 1a) over 100 years ago [*Jaggar*, 1920], and a telemetered electronic seismic network was first installed in the late 1950s and has been steadily growing and improving ever since [*Eaton and Murata*, 1960; *Klein and Koyanagi*, 1980; *Klein et al.*, 1987; *Kauahikaua and Poland*, 2012]. The current network operated by the U.S. Geological Survey (USGS) Hawaiian Volcano Observatory (HVO) (Figure 1a) records approximately 5000–10,000 seismic events per year [*Nakata*, 2007; *Nakata and Okubo*, 2010]. Seismicity has played a central role in developing models of how Hawaiian volcanoes work [e.g., *Eaton and Murata*, 1960; *Eaton*, 1962; *Klein et al.*, 1987; *Ryan*, 1988; *Tilling and Dvorak*, 1993; *Wright and Klein*, 2006; *Got et al.*, 2008].

[3] Significant improvements in the relative location accuracy among nearby seismic events can be achieved without solving directly for the biasing effects of three-dimensional (3-D) velocity heterogeneity [e.g., *Douglas*, 1967; *Frohlich*, 1979; *Fréchet*, 1985; *Got et al.*, 1994; *Shearer*, 1997; *Richards-Dinger and Shearer*, 2000; *Waldhauser and Ellsworth*, 2000; *Lin and Shearer*, 2005]. Relative relocation can achieve high location precision using differential times obtained via waveform cross correlation [e.g., *Fréchet*, 1985; *Got et al.*, 1994; *Fremont and Malone*, 1987; *Nadeau et al.*, 1995; *Waldhauser et al.*, 1999; *Shearer et al.*, 2005; *Lin et al.*, 2007], in many cases collapsing diffuse seismicity to compact streaks aligned with fault slip [*Rubin et al.*, 1999] or to planar surfaces reflecting fault planes [*Got et al.*, 1994]. Relative relocation techniques have been used extensively to study seismicity on Hawaii Island; however, most studies have focused on subregions of the island or specific event sequences or types [e.g., *Got et al.*, 1994; *Gillard et al.*, 1996; *Got and Okubo*, 2003; *Battaglia*

Additional supporting information may be found in the online version of this article.

[1]Institute of Geophysics and Planetary Physics, Scripps Institution of Oceanography, University of California, San Diego, La Jolla, California, USA.

[2]Division of Marine Geology and Geophysics, Rosenstiel School of Marine and Atmospheric Science, University of Miami, Miami, Florida, USA.

[3]Hawaii Institute of Geophysics and Planetology, University of Hawaii at Manoa, Honolulu, Hawaii, USA.

[4]Now at Earthquake Hazards Program, U.S. Geological Survey, Reston, Virginia, USA.

[5]Hawaiian Volcano Observatory, U.S. Geological Survey, Hawaii Volcanoes National Park, Hawaii, USA.

Corresponding author: R. S. Matoza, Institute of Geophysics and Planetary Physics, Scripps Institution of Oceanography, University of California, San Diego, 9500 Gilman Dr., La Jolla, CA 92093-0225, USA. (rmatoza@ucsd.edu)

2169-9313/13/10.1002/jgrb.50189

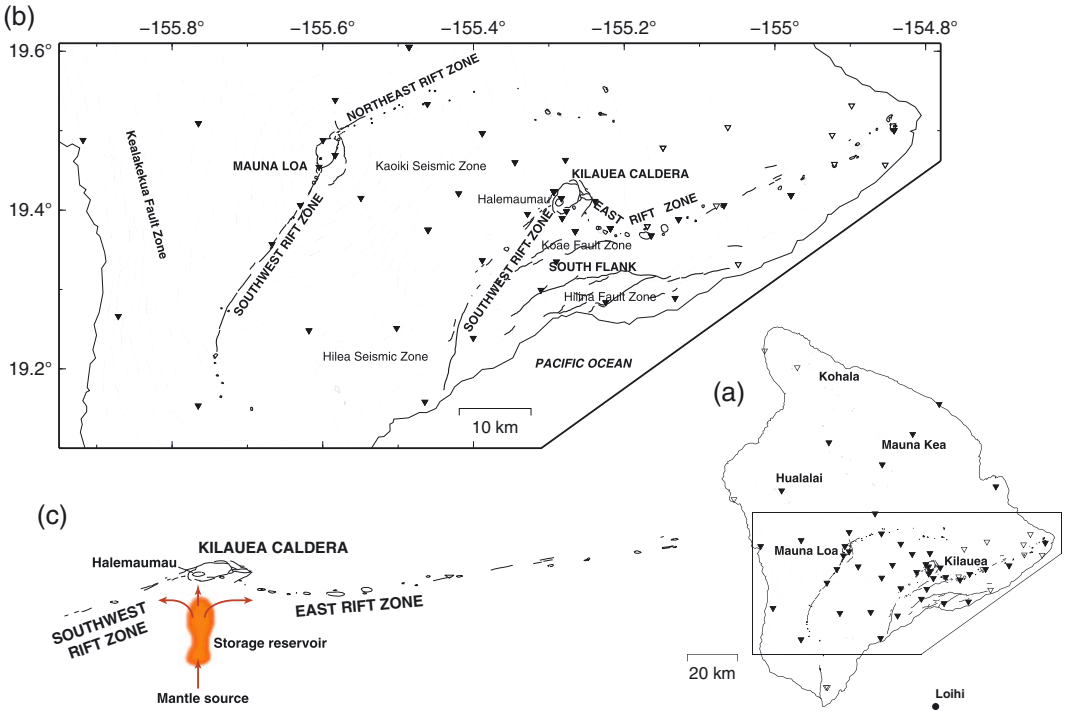

Figure 1. (a) Map of the island of Hawaii showing the locations of volcanoes (Kilauea, Mauna Loa, Mauna Kea, Hualalai, Kohala, and Loihi seamount), major faults and craters, and 60 seismic stations operated by the USGS HVO and the NOAA PTWC from which data were considered in this study (inverted triangles) [*Nakata and Okubo*, 2010]. Solid black inverted triangles are stations recording at least 30% of all events considered. Contour interval is 300 m. Polygon indicates area of Figure 1b. (b) Expanded view of region in Figure 1a showing the principal morphological and seismic features of Kilauea and Mauna Loa volcanoes discussed in the text. Contour interval is 200 m. (c) Schematic of Kilauea's magma system (after *Tilling and Dvorak* [1993]), including a mantle source, a pathway of magma transport up from the mantle, a shallow (2–6 km) subcaldera storage reservoir marked by low seismicity and deformation centroids of inflation and deflation, and shallow lateral distributaries from this reservoir into two rift zones to the east and southwest.

et al., 2003; *Wolfe et al.*, 2003, 2004; *Okubo and Wolfe*, 2008; *Yamada et al.*, 2010].

[4] The aim of the present work is to produce a comprehensive and systematically relocated multiyear catalog of seismicity recorded by the HVO permanent network. We apply waveform cross correlation and cluster analysis techniques similar to those developed for relocating seismicity in southern California [*Shearer et al.*, 2005; *Lin et al.*, 2007] to the HVO data set from January 1992 to March 2009, which includes seismicity both beneath Hawaii Island and offshore. Our results show a dramatic sharpening of seismicity patterns, which permit a more detailed understanding of fault geometries and volcanic and tectonic processes.

2. Context: Seismicity on Hawaii Island

[5] Seismicity in this intraplate setting ultimately results directly or indirectly from volcanism [*Eaton*, 1962]. The majority of seismicity recorded by the HVO network is concentrated around and beneath the active summits and rift zones of the basaltic shield volcanoes Kilauea and Mauna Loa and the Loihi seamount (Figures 1a and 1b). Seismicity also occurs on mobile flanks and fault systems accommodating stress from repeated intrusions and gravitational instability from volcano growth [e.g., *Swanson et al.*, 1976; *Got et al.*, 1994; *Owen et al.*, 1995; *Got and Okubo*, 2003; *Segall et al.*, 2006a; *Brooks et al.*, 2006]. Additional earthquakes around and beneath Hawaii Island (e.g., the 2006 M_w 6.7 Kiholo Bay earthquake; *Yamada et al.*, [2010]) appear to be related to lithospheric flexure and subsidence of the entire island due to volcano loading, with additional stresses of magmatic origin probably contributing at shallower depths [*Klein et al.*, 1987; *Wolfe et al.*, 2003, 2004; *Pritchard et al.*, 2007; *McGovern*, 2007]. A significant fraction of deeper ($\geq$13 km) seismicity is clustered along low-angle planes interpreted as preexisting fault zones in the lower crust and upper mantle [*Wolfe et al.*, 2003, 2004].

[6] Kilauea's magmatic system (Figure 1c) has been the most active and studied since the establishment of seismic monitoring [*Eaton and Murata*, 1960; *Klein et al.*, 1987; *Ryan*, 1988; *Tilling and Dvorak*, 1993; *Wright and Klein*, 2006]. Historical eruptions have occurred either within the summit area (usually at the Halemaumau pit crater) or along either rift zone, with rift zone eruptions fed directly either from the summit or from secondary reservoirs along a rift zone [*Tilling and Dvorak*, 1993].

[7] Diverse seismic signals result from a variety of processes associated with this magma transport system and

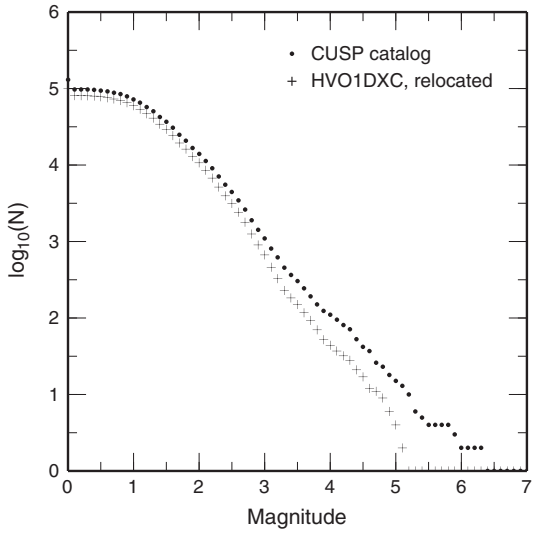

Figure 2. Gutenberg-Richter magnitude-frequency plot for the original 130,902 events we considered (CUSP catalog) and 101,390 events relocated using a 1-D velocity model, waveform cross correlation, and cluster analysis (HVO1DXC). *N* is the number of events with magnitude greater than or equal to magnitude *M*. The relocation procedure is biased toward more frequently occurring, lower magnitude seismicity.

include, for example, (1) volcano-tectonic (VT) earthquakes, which are ordinary earthquakes in the brittle volcanic edifice or crust resulting from magmatic processes; (2) larger ($M > 4.4$) earthquakes and their aftershock sequences [*Wright and Klein*, 2006]; (3) "deep" long-period (DLP) events and tremor in the mantle at ∼35–60 km depth beneath Kilauea associated with deep magma transport [*Eaton and Murata*, 1960; *Aki and Koyanagi*, 1981; *Koyanagi et al.*, 1987; *Shaw and Chouet*, 1989]; (4) long-period (LP) seismic events associated with a shallow hydrothermal system near Halemaumau pit crater within the summit caldera of Kilauea [*Saccorotti et al.*, 2001; *Almendros et al.*, 2001; *Kumagai et al.*, 2005]; and (5) VT swarms, shallow tremor, LP, and very long period (VLP) seismicity associated with magmatic degassing and summit and rift zone eruptions [e.g., *Swanson et al.*, 1979; *Klein et al.*, 1987; *Ferrazzini et al.*, 1991; *Chouet*, 1996a; *Ohminato et al.*, 1998; *Chouet et al.*, 2010; *Dawson et al.*, 2010; *Chouet and Dawson*, 2011; *Patrick et al.*, 2011]. We note that studies of LP and VLP seismicity have often used additional array or broadband deployments [e.g., *Dawson et al.*, 1998], which we do not consider in this work.

[8] Figure 1b shows the major mapped fault systems of Kilauea and Mauna Loa. Kilauea is buttressed to the west and north by the enormous Mauna Loa Volcano and has grown on its south flank, such that Kilauea's growth and deformation are primarily accommodated to the south [*Swanson et al.*, 1976]. Kilauea's south flank (Figure 1b) is sliding seaward at an average rate of ∼6–10 cm/yr along a crustal detachment fault (décollement) separating the volcanic edifice and old oceanic crust at ∼7–11 km depth [*Swanson et al.*, 1976; *Got et al.*, 1994; *Owen et al.*, 1995, 2000; *Got and Okubo*, 2003; *Hansen et al.*, 2004]. Kilauea's south flank is delimited by the Koae Fault Zone, the southwest rift zone (SWRZ), and east rift zone (ERZ) (Figure 1b); these three dilating systems are viewed as forming the tearaway zone for Kilauea's mobile south flank [*Swanson et al.*, 1976]. Detachments along Kilauea's and Mauna Loa's south flank are the inferred source of large damaging earthquakes which have generated tsunamis—the 1868 $M \sim 7.9$ Great Ka'u and 1975 *M* 7.2 Kalapana earthquakes. The possibility of catastrophic south flank collapse has been suggested to represent an even greater tsunami hazard [*Moore et al.*, 1994; *Ward*, 2002].

[9] Kilauea's south flank motion results from a combination of forceful dike intrusion in the rift zones and gravitational sliding; however, their relative contributions are currently unresolved [*Swanson et al.*, 1976; *Owen et al.*, 2000]. Continuous GPS data on Kilauea's south flank have recorded slow-slip events (SSEs) within the offshore extension of the Hilina Slump (south of the Hilina Fault Zone, Figure 1b), which represent an intermediate behavior between stable aseismic sliding and unstable stick slip and are analogous to SSEs in subduction zones [*Cervelli et al.*, 2002; *Brooks et al.*, 2006; *Segall et al.*, 2006a; *Syracuse et al.*, 2010; *Montgomery-Brown et al.*, 2009]. The depths of the SSEs are difficult to determine from geodetic data alone, and thus relocated triggered microseismicity has been used to constrain their depth [*Segall et al.*, 2006a, 2006b; *Wolfe et al.*, 2007; *Syracuse et al.*, 2010].

[10] At Mauna Loa, low-angle detachments similar to that inferred beneath Kilauea's south flank have been inferred on the west (Kealekekua Fault Zone) and southeast (Hilea and Kaoiki seismic zones) flanks (Figure 1b) [*Wolfe et al.*, 2004]. Seismicity in the Kaoiki and Hilea seismic zones (Figure 1b) reflects complex mechanical interactions between Mauna Loa and Kilauea volcanoes; seismicity in these areas includes a combination of detachment and strike-slip mechanisms [*Klein et al.*, 2001; *Got and Okubo*, 2003; *Walter and Amelung*, 2004]. Two swarms of DLPs occurred in the mantle beneath Mauna Loa in 2002 (31 events) and 2004–2005 (∼2000 events) associated with a geodetically observed intrusion [*Okubo and Wolfe*, 2008].

3. Data

3.1. HVO Waveform Data and Catalog

[11] We consider data from the USGS HVO permanent telemetered seismic network and additional stations operated by the National Ocean and Atmospheric Administration (NOAA) Pacific Tsunami Warning Center (PTWC) as described by *Nakata and Okubo* [2010]. The standard stations are 1 Hz short-period geophones and the majority are vertical component only; all stations use analog FM telemetry. We obtained event-triggered waveform data in CUSP/XDR format for 130,902 events from January 1992 to March 2009. The waveform data are from 60 unique station locations on Hawaii Island; 46 stations had waveform data available for at least 30% of the events considered and are likely to contribute most to the relative relocation results (Figure 1a). The starting catalog of hypocenters and magnitudes for the 130,902 events was produced at HVO using the CUSP processing platform and a one-dimensional (1-D) velocity model. The catalog is considered complete down to a magnitude of about 1.5 (Figure 2). The CUSP catalog used

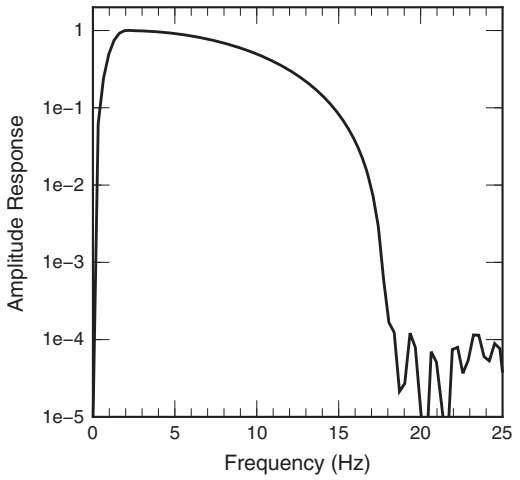

Figure 3. Response of the 1-10 Hz filter applied to the waveform data prior to cross correlation. The response (logarithmic y scale) rolls off gently toward high frequencies, retaining energy up to about 15 Hz.

for our starting locations is slightly different from the final locations published by HVO for only a high-quality subset of the triggered events [e.g., *Nakata and Okubo*, 2010]; however, we use the CUSP catalog as we need a starting location for every event in our waveform database. Both P and S phase-pick data were available for a subset of about 53,000 events.

3.2. Preprocessing

[12] We convert the waveform data to a custom Event Filing System (EFS) binary format in a year/month directory structure, requiring a total of 223 GB of storage. EFS files contain all the waveform, event, station, and phase-pick information for a single event, greatly reducing the total number of files in large databases and speeding input/output. We then resample the data to a uniform 100 Hz sample rate and band-pass filter between 1 and 10 Hz (Figure 3). Filtering is performed all at once, creating a separate archive of EFS filtered waveform data. We note that the 1–10 Hz filter has a gentle roll-off at high frequencies, retaining energy up to about 15 Hz (Figure 3).

4. Relative Relocation

[13] We use methods similar to those developed for relocating seismicity in southern California [*Shearer et al.*, 2005; *Lin et al.*, 2007], but with some significant improvements to the algorithms. Our final product, which we call HVO1DXC, is the result of relative relocation only (sections 4.1 and 4.2); events that group into similar event clusters are relocated relative to the other events within the cluster; however, the absolute location of the cluster centroid remains constrained by the CUSP catalog hypocenters. In addition, the starting locations for the relative relocation procedure are the CUSP catalog locations. The cross correlations and relative relocations are performed using a 1-D velocity model (a smoothed version of the *Klein* [1981] model; Figure 4) and do not take into account topography. Because we use a 1-D velocity model and do not take into account station elevation, the depth datum is approximately the mean station elevation (∼1.5 km above sea level (asl) for the 46 stations recording at least 30% of all events; Figure 1a). We acknowledge that this is not ideal for Hawaii Island, which has more topography than southern California, and plan to take topography into account in future improvements to the Hawaiian catalog.

[14] The frequency band pass (section 3.2) and parameters we use in the waveform cross-correlation procedure (see section 4.1) are similar to those used in southern California [*Shearer et al.*, 2005; *Lin et al.*, 2007]. These parameters are suitable for ordinary volcano-tectonic (VT) events. However, the HVO data set also includes long-period (LP) (0.5–5 Hz) events [e.g., *Chouet*, 1996b; *Okubo and Wolfe*, 2008], and some LP events do correlate and relocate using our chosen parameters, even though they are not optimal for LP events. HVO analyst identification and classification of LP events have not been systematic during the time period considered, so we cannot currently separate the LP events from the rest of the seismicity in the catalog. Therefore, LP events are included in our final catalog HVO1DXC, but their locations are considered suboptimal.

4.1. Waveform Cross Correlation

[15] Following *Shearer et al.* [2005] and *Lin et al.* [2007], we pair each event with all events that fall within a 2 km radius using initial catalog locations. If at least 100 events are not found within 2 km, we use Delaunay tessellation to find at least 100 nearest neighbors [*Richards-Dinger and Shearer*, 2000]. The number of pairs for each event therefore varies between 100 and a very large number, depending upon the density of seismicity. In total, we consider ∼45.5 million event pairs.

[16] For every pair, we compute waveform cross correlation separately for P and S phases on all available stations and components. We compute the cross-correlation

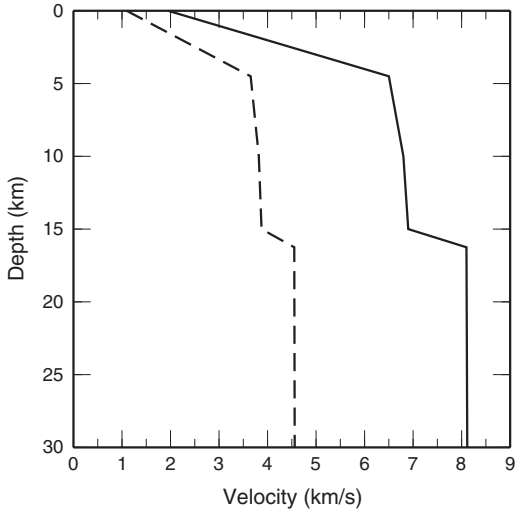

Figure 4. The 1-D velocity model used in this study (V_p, solid line; V_s, dashed line) shown for 0–30 km. The model is a smoothed and interpolated version of the *Klein* [1981] model. The *Klein* [1981] model is used in the routine HVO catalog hypocenter location after linear interpolation as described by *Nakata and Okubo* [2010]. The velocity model is available in the supporting information.

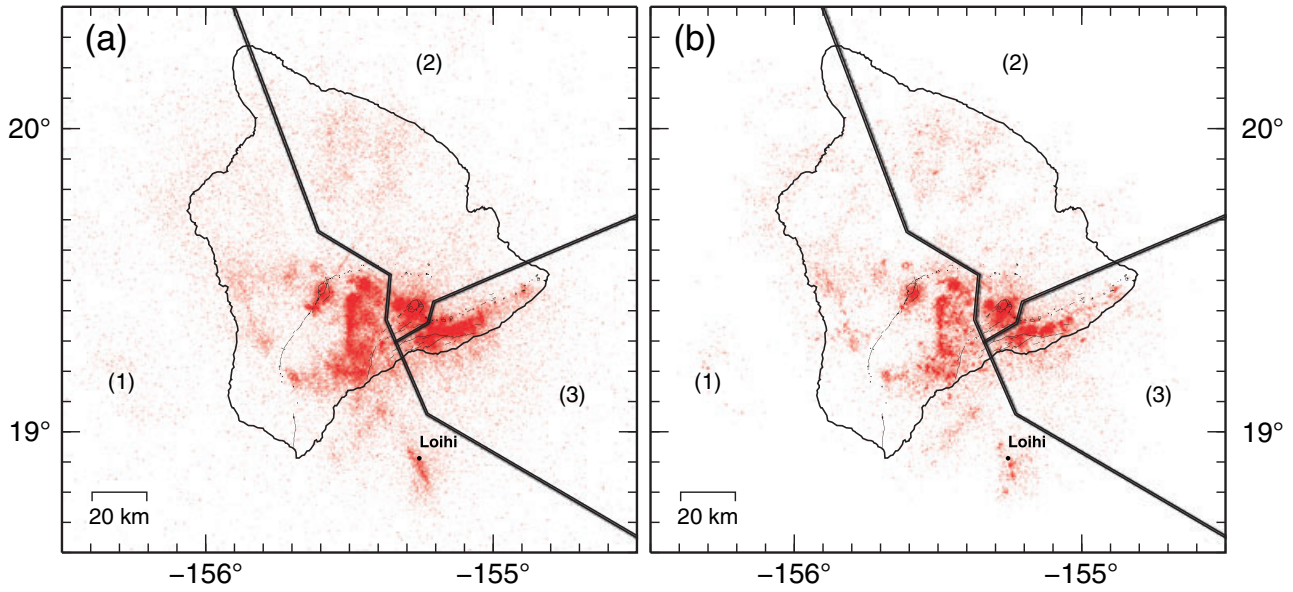

Figure 5. Seismicity from January 1992 to March 2009 (a) before and (b) after relocation with a 1-D velocity model, waveform cross correlation, and cluster analysis. (a) CUSP catalog locations for the 130,902 events considered. (b) Locations for the 101,390 relocated events (HVO1DXC). In both plots, we show the boundaries of the three polygons [(1), (2), (3)] used to divide the seismicity into subsets for efficient processing.

functions using symmetric time shifts of up to ±1.5 s and waveform time windows defined as follows: (1) if *P* picks are available, the *P* window is –0.5 s to 1 s around the *P* pick (1.5 s window), and the *S* window is –1 s to 2 s (3 s window) around a theoretical *S* pick defined as the *P*-pick time plus the theoretical *S*–*P* time; or (2) if *P* picks are not available, we use –1 s to 1 s (2 s window) around a theoretical *P* pick and –0.5 s to 1.5 s (2 s window) around a theoretical *S* pick. The theoretical picks are calculated using travel time tables computed from the 1-D velocity model (Figure 4), together with the CUSP catalog location and origin time. Spline interpolation is used to obtain differential time measurements with a nominal precision of 1 ms. Because there may be cross-correlation measurements of the same phase from different components of the same station, we remove the redundancy by favoring *P* measurements from the vertical component and *S* measurements from the horizontal components, and then selecting the measurement with the highest correlation. We do not use negative cross-correlation results in the subsequent relocation steps; therefore, reversed polarity stations and phase shifts across the focal sphere are not taken into account in the relocation algorithm.

[17] We only save waveform cross-correlation results for the ∼32 million pairs that have an average *P* and *S* waveform correlation coefficient >0.45 and at least eight differential time measurements with correlation coefficient >0.65 from source-station distances <80 km. The distance cutoff is adopted because seismograms from distant stations tend to have lower frequencies and give higher correlations [*Shearer et al.*, 2005]. The distance cutoff is only for deciding whether to save the event pair information. If the aforementioned criteria are satisfied for a given event pair (i.e., the pair is defined as similar), we use all differential times for the pair from cross correlations with correlation coefficient >0.6, including stations at greater distance. We note that the correlation coefficient value depends on the time-bandwidth product of the cross correlation, which is related to the band pass 1–10 Hz and cross-correlation window length (1.5 s and 3 s for *P* and *S* waves, respectively, if *P* picks available and 2 s if *P* picks not available). Our waveform cross-correlation parameters and threshold criteria to use the cross-correlation results were developed and tested on southern California data sets [e.g., *Lin et al.*, 2007].

[18] The band pass of 1–10 Hz (Figure 3) used for the cross correlation has been used in previous relocation studies in southern California [*Lin et al.*, 2007]. The filter retains energy up to ∼15 Hz (Figure 3). Because small-magnitude seismicity may have dominant frequencies approaching or exceeding 10 Hz, we tested for potential effects of the choice of filter on a group of 3154 events, approximately corresponding to the events shown in Figure 10. We re-filtered the waveforms of these events with a separate 1–20 Hz band-pass filter and recomputed cross correlations following the procedure described above. We found that 92% of the cross-correlation times (corresponding to correlation coefficients >0.6) change less than 0.05 s when we use the 1–20 Hz filter instead of the 1–10 Hz filter. However, we also found that significantly less "good" correlations were found (i.e., the correlation coefficients were lower) when using the 1–20 Hz filter, probably because of additional noise in the 10–20 Hz band. Additionally, during the cross-correlation procedure, some degree of cycle skipping does occur. In principle, a method to detect and remove cycle skipping would be worthwhile, but we have not implemented such a method for the current version of the catalog. However, by using the $L1$-norm, our results should be reasonably robust with respect to any large travel time errors introduced by cycle skipping.

4.2. Cluster Analysis and Relocation

[19] To facilitate memory handling and speed up the subsequent calculations, we divide the seismicity along natural spatial breaks in the seismicity into three slightly overlapping polygons (Figure 5) following *Hauksson and Shearer* [2005] and *Shearer et al.* [2005]. The processing steps described in this section are performed separately for each polygon. At the end of the relocation procedure, the results from the three polygons are recombined. For 923 relocated events that fall into more than one polygon, we keep the relocation result that uses the greater number of differential time pairs.

[20] In previous relocation studies for southern California [*Shearer et al.*, 2005; *Lin et al.*, 2007; *Hauksson et al.*, 2012], the waveform cross-correlation results were used to relocate the events by first identifying similar event clusters using cluster-analysis, and then separately relocating the events within each cluster using an iterative location method. In both stages, a minimum correlation-coefficient cutoff is used to define similar waveforms, similar event pairs, and "good" differential times, but above this threshold, more highly correlated data do not receive greater weight. In addition, the iterative method for relocating events within a given similar event cluster is computationally intensive for large clusters (e.g., more than 100 events) and may be slow to converge in cases where valid differential times are available for only a fraction of the possible event pairs in the cluster.

[21] Motivated by these shortcomings, we have developed a new relocation method, termed GrowClust, that combines the cluster analysis and relocation stages into a single algorithm. Our approach is also motivated by computational efficiency. We wish to achieve high location precision for a large number of events, without inverting very large matrices, e.g., by avoiding inverting all differential times all at once. The new approach starts by identifying and relocating the most highly correlated events first and then keeps the relative locations of these events fixed while successively relocating additional events with respect to the currently defined clusters, similar to the method described by *Got et al.* [1994] and *Got and Okubo* [2003]. More specifically, GrowClust works as follows:

[22] 1. It begins by defining every event as a cluster of one event with an initial (CUSP catalog) location.

[23] 2. For every event pair, a similarity coefficient is defined as the number of similar waveform pairs (either *P* or *S* phases) for stations within 80 km and with correlation coefficients above 0.6, multiplied by their average correlation coefficient. We note, however, that GrowClust considers all differential time measurements with correlation coefficient >0.6, including for stations at greater distance.

[24] 3. It sorts the similarity coefficients in descending order, from the most similar event pair to the least similar event pair. The algorithm then works its way through all the event pairs, starting with the most similar. For each event pair, there are three possibilities: i. Both events are members of single-event clusters. In this case it combines the two clusters into a new cluster with two members. It performs relative location of the two events about their average location, using a grid-search $L1$-norm method [see *Shearer et al.*, 2005]. ii. Both events are part of the same cluster. In this case, the algorithm does nothing because they should already have been relocated. iii. One or both events are part of a multi-event cluster. In this case, the algorithm first finds other event pairs linking the two clusters. To combine the clusters, it requires that the ratio of the number of these pairs to the total number of possible pairs linking the two clusters exceeds a specified threshold (0.005, or 0.5% for the results presented here). If the threshold is exceeded, it attempts to relocate the clusters with respect to each other, using the 10 event pairs with the highest similarity coefficients (or all available pairs if there are less than 10). In doing so, it keeps the relative locations of the events within each starting cluster fixed; it moves only the two cluster centroids about the centroid of the combined cluster. Again, it uses a grid-search $L1$-norm method, generalized in this case to consider multiple-event data, but remaining computationally efficient because it is effectively solving only for a single differential location between the cluster centroids. In order to stop clusters from drifting too far from their original absolute locations, we define maximum allowable shifts in cluster centroids resulting from this relocation step. For clusters with more than 10 events, the algorithm checks to see if the cluster centroid has moved by more than 1 km and 2 km in the horizontal and vertical directions, respectively. If the cluster centroid shift exceeds either maximum allowed cutoff, the attempt to merge the clusters is rejected.

[25] 4. The algorithm continues until no more clusters can be combined and relocated, given the cutoff requirements. Only clusters with at least five events are saved.

[26] In step 3-iii above, we defined maximum allowable shifts in cluster centroids. These distance cutoff criteria were implemented based on early experiments with the algorithm. In the experiments, we found that spurious results are sometimes generated from a small number of cross-correlation measurements linking distant clusters. Implicit in relative relocation methods is the assumption that the relative shifts in location are small. If the shifts are large, the linearization of the problem is exceeded, leading to spurious results. Our distance cutoff criteria therefore act to prevent clusters that are considered too far apart from linking together, causing location shifts that exceed the assumed linear approximation. The values of 1 km and 2 km in the horizontal and vertical directions, respectively, reflect the a priori knowledge that the horizontal (latitude and longitude) location of the events is better constrained than the depth in the original CUSP catalog locations.

[27] In total, this procedure groups and relocates 101,390 events (77% of all events considered) in 772 different similar event clusters. This approach has the advantage that the best correlated data are relocated first, and these relative locations are preserved when less correlated data are added. The method is much faster computationally than the *Lin et al.* [2007] algorithm for large data sets. We have validated this combined clustering and location method on simple synthetic data sets.

4.3. Relative Location Uncertainties

[28] As described above, the GrowClust algorithm achieves relocation progressively, relocating a cluster of events with respect to another cluster of events and then combining them while preserving the relative locations within each cluster (step 3-iii above). This approach is different from that described by *Lin et al.* [2007], where similar event clusters are defined prior to any relocation and then

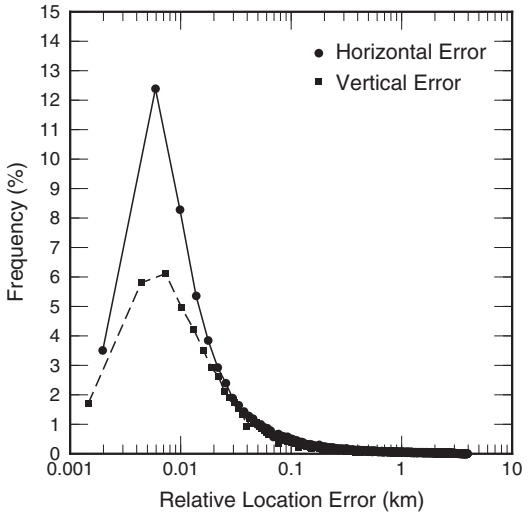

Figure 6. Histograms of formal relative location errors estimated by bootstrapping. For the horizontal errors (circles, solid line), the 5th, 25th, 50th, 75th, and 95th percentiles are 4 m, 12 m, 64 m, 544 m, and 2248 m, respectively. For the vertical errors (squares, dashed line), they are 4 m, 16 m, 71 m, 516 m, and 1758 m, respectively.

relocation is performed globally and iteratively for all events within the cluster. In the *Lin et al.* [2007] algorithm, estimating formal relative location uncertainties is relatively simple via a bootstrap approach, in which differential times for each event are randomly resampled. In the GrowClust approach, estimating relative location uncertainties is not straightforward and is beyond the scope of the present work.

[29] In order to provide some measure of relative location uncertainty, we use the relocation results from GrowClust as starting locations in the original relocation algorithm of *Lin et al.* [2007]. This enables stability tests of the relocation results and allows us to estimate formal relative location uncertainties for the relocated events. We apply the grid-search relocation algorithm described by *Lin et al.* [2007] with 10 iterations and using the $L1$ norm.

[30] We estimate formal relative location uncertainties using the bootstrap approach described by *Lin et al.* [2007] (Figure 6). Differential times for each event are randomly resampled, and the event is relocated using the resampled differential times. We repeat this 20 times for each event, and the formal vertical and horizontal relative location uncertainties (Figure 6) are calculated from the standard deviations of these 20 samples. For the horizontal errors, the 5th, 50th, and 95th percentiles are 4 m, 64 m, and 2248 m, respectively. For the vertical errors, they are 4 m, 71 m, and 1758 m, respectively.

[31] We note that 20 bootstrap samples is too small a number to fully sample the statistical distribution. As explained by *Lin et al.* [2007], we consider our bootstrap uncertainties to be an approximation to the underlying distribution. Using a greater number of samples (e.g., 1000 samples were used by *Got et al.* [1994] and *Got and Okubo* [2003]) would lead to more accurate uncertainties, but at a much greater computational cost given the large number of events we consider. Furthermore, the quoted uncertainties only reflect the distribution of errors due to data sampling (i.e., assessing the effect of including or not including particular differential time measurements). The uncertainties in Figure 6 do not reflect the uncertainties due to velocity structure or topography that are likely greater.

[32] Applying the *Lin et al.* [2007] relocation algorithm to our locations obtained with GrowClust results in a separate solution for the seismicity locations (not shown here), which provides an independent validation of our relocation algorithm. We deduce that our main results are robust with respect to the location method because the relative seismicity patterns obtained with GrowClust change only slightly when applying the *Lin et al.* [2007] algorithm.

4.4. Absolute Location Uncertainty

[33] Although our method considerably improves relative locations between nearby events, the absolute locations of cluster centroids remain constrained by the original CUSP catalog locations and will contain errors resulting from topography and unknown 3-D velocity structure. For example, a change in the velocity model or unmodeled 3-D velocity structures could rotate the ray parameters, therefore rotating the relative relocations. This should be kept in mind when interpreting our relocations, for example, in terms of the depths, dips, and geometry of inferred décollements (discussed further in section 5.2). In general, we expect the original catalog locations to be more accurate in latitude and longitude than in depth, since depth is more sensitive to the velocity model used.

[34] In order to illustrate potential effects of 3-D velocity structure on the absolute locations, we compare our relocations with a subset of the 53,000 events with phase-pick data relocated by *Lin et al.* [2012] using a 3-D velocity model. Our method described in sections 4.1 and 4.2 utilizes the available phase-pick data only in defining time windows for waveform cross correlation. In a separate study, *Lin et al.* [2012] used the phase-pick data to improve absolute and relative earthquake locations simultaneously by combining 3-D ray tracing with the source-specific station term (SSST) method, following similar approaches as in *Lin et al.* [2007]. *Lin et al.* [2012] relocate 45,784 events, which we refer to here as "3-D locations."

[35] We make comparisons between our HVO1DXC results and the 3-D locations from *Lin et al.* [2012] as follows. For each similar event cluster in the HVO1DXC results, we identify events within the cluster that also have an independent 3-D location. If at least 10 events and 20% of all events in the cluster have independent 3-D locations (i.e., were relocated separately by *Lin et al.* [2012]), we shift the cluster. In this case, we shift the cluster centroid so that it aligns with the centroid of the corresponding 3-D locations. Thus, we use the 3-D locations of *Lin et al.* [2012] to adjust the absolute locations of our clusters without changing their relative locations. This adjustment of absolute locations also causes a change in the depth datum used for the seismicity. As stated in the introduction to section 4, the depth datum for the HVO1DXC catalog is approximately the mean station elevation ($\sim$1.5 km asl). However, in the 3-D locations of *Lin et al.* [2012], the depth datum is mean sea level. Thus, there is a vertical shift of $\sim$1.5 km in absolute depth resulting from the depth datum change between the two location methods. Analyses of these results are presented in section 5.2.

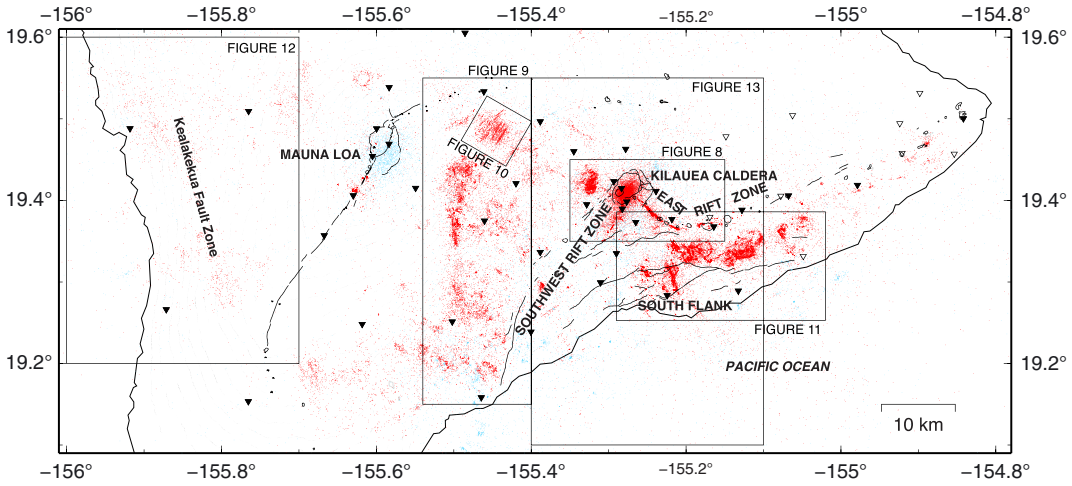

Figure 7. Relocated HVO1DXC seismicity, with boxes indicating areas of Figures 8–13. Events with depths ≥13 km are shown in cyan. Inverted triangles are seismic stations; solid black inverted triangles are stations recording at least 30% of all events considered. Contour interval is 300 m.

5. Relocation Results

[36] The final relocations are available in the supporting information as the HVO1DXC catalog. Figure 7 shows the HVO1DXC relocated seismicity around Kilauea and Mauna Loa. A comprehensive analysis of the relocated seismicity and its implications is beyond the scope of this paper. However, in this section, we highlight some main features of our relocation results in chosen focus regions (boxes in Figure 7).

5.1. Kilauea Summit Region

[37] Seismicity in the Kilauea summit region, including the upper SWRZ and ERZ, is particularly well resolved because of the dense station coverage in this area (Figures 1 and 8). Seismicity in the northwest area of Figure 8b is related to the Kaoiki Fault Zone [*Neal and J. P. Lockwood* 2003] and contains sharp earthquake streaks that were previously identified by *Rubin et al.* [1999], which are not resolvable in the original CUSP catalog locations (Figure 8a). Streaks of seismicity at ∼3 km depth are associated with the upper SWRZ and upper ERZ. The band of seismicity in the upper SWRZ does not align along the surface expression of the rift, but "heads south from the caldera for about 3 km before bending to the southwest" [*Klein et al.*, 1987]. Seismicity streaks beneath the upper ERZ were studied in relocation work by *Gillard et al.* [1996], who interpreted the locations and focal mechanisms as reflecting left-lateral motion of the deep rift system in response to southeasterly displacement of the south flank. Note that *Gillard et al.* [1996] considered 826 events that occurred in 1991, which does not overlap with our data time period. Our relocation results include >5000 events in the upper ERZ band of seismicity, and we recover an overall spatial and depth distribution similar to that of *Gillard et al.* [1996]. *Gillard et al.* [1996] obtain two distinct bands of seismicity, whereas our results show a single, more continuous, band. These differences in results could be due to differences in accuracy between the methods as well as differences in the events

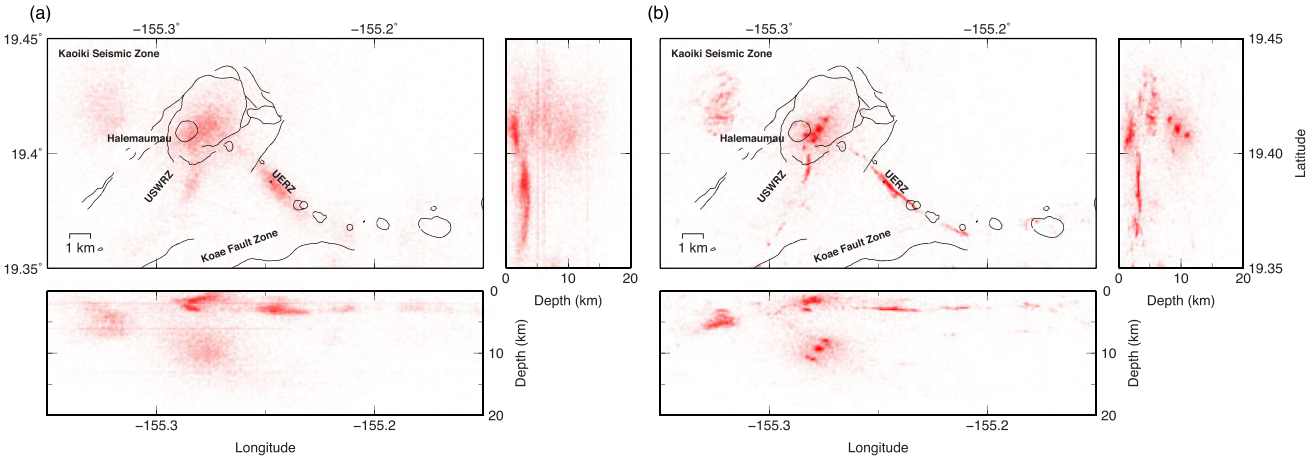

Figure 8. Seismicity in the Kilauea summit region (see Figure 7) for (a) original CUSP catalog locations and (b) relocated catalog, HVO1DXC. The right and bottom plots in each case only show seismicity occurring in the latitude and longitude window of the top-left plot. USWRZ: Upper South West Rift Zone, UERZ: Upper East Rift Zone.

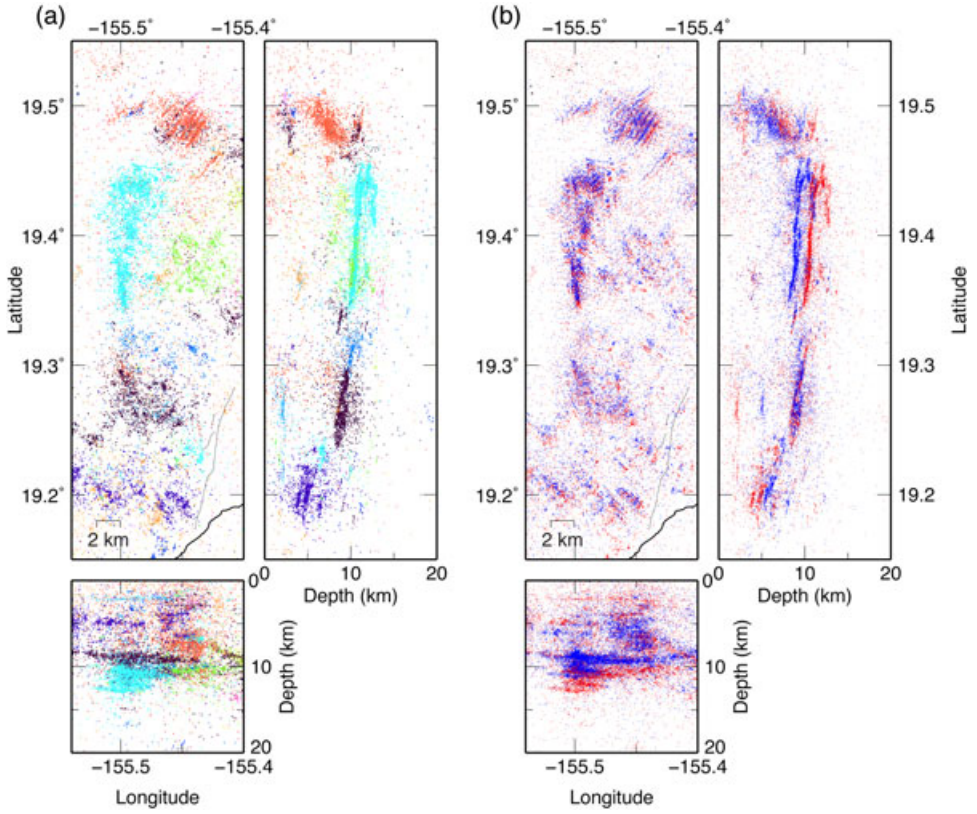

Figure 9. Seismicity in the region between Mauna Loa and Kilauea summits (see Figure 7). (a) HVO1DXC relocated seismicity, with colors used to highlight the different clusters (color scale arbitrary). (b) HVO1DXC relocated seismicity (red dots; same as in Figure 9a) and the same events shifted to correspond with 3-D locations (blue dots; see section 4.4 for more details).

considered, since our data time period does not overlap with that of *Gillard et al.* [1996].

[38] Our relocations also include seismicity in tight clusters at shallow depth (0–5 km) beneath Kilauea caldera and east of Halemaumau (Figure 8b). An additional three distinct spatial clusters of seismicity are found at depths of ∼8, 9, and 11 km beneath the area east of Halemaumau (Figure 8b). These events are also temporally clustered, occurring with swarm-like behavior, and with different spatial locations active at different times. This region broadly corresponds to the region of LP events relocated by *Battaglia et al.* [2003]; however, as discussed in section 4, LP events have not been comprehensively identified, and our method is not designed for LP events, so their locations are likely suboptimal.

5.2. Region Between Mauna Loa and Kilauea

[39] The region between Mauna Loa and Kilauea (Figure 9) is a good place to illustrate the effects of relative versus absolute location uncertainty. Figure 9a shows the HVO1DXC seismicity with different similar-event clusters plotted in different colors. Our method (section 4) improves the relative location accuracy between events within a given cluster (i.e., events of the same color), but the positions of the different clusters with respect to each other are less well constrained. The seismicity in Figure 9a forms a sharp, planar surface at ∼10 km depth, consistent with seismicity resulting from a detachment or décollement fault [*Got and Okubo*, 2003]. The collapsing of diffuse seismicity into a planar surface in depth is a robust result of our relocation procedure. However, the dip of the surface across the full latitude range of ∼19.2°–19.5° in Figure 9a is not well constrained by our procedure, because the seismicity is divided into different clusters. Therefore, we cannot be certain that the apparent northward dip of the surface from ∼19.2° to 19.5° is a robust result. A single cyan-colored cluster centered on ∼19.4° also has a gentle northward dip; however, the dip of this cluster could be affected by unmodeled 3-D velocity structure. The gentle northward dip of seismicity in this region is consistent with previous relocation work by *Got and Okubo* [2003], probably because we use a similar 1-D velocity model.

[40] In Figure 9b, we compare our relocated seismicity with the same seismicity shifted to align with the independently derived 3-D locations (section 4.4). The difference in the two sets of solutions shown in Figure 9b illustrates one potential effect of adding information about the 3-D velocity structure and topography (blue dots) versus our procedure using a 1-D velocity model (red dots). In addition to the overall dip of the seismicity changing slightly from the shift in cluster centroids, Figure 9b indicates that the absolute depth of the seismicity could be ∼2 km shallower than it appears in our HVO1DXC catalog (note that ∼1.5 km of this depth change results from the difference in depth datum between the 1-D and 3-D location methods). We present these comparisons as a caution against over interpreting the absolute locations (particularly the depths and dips) in our relocated seismicity catalog.

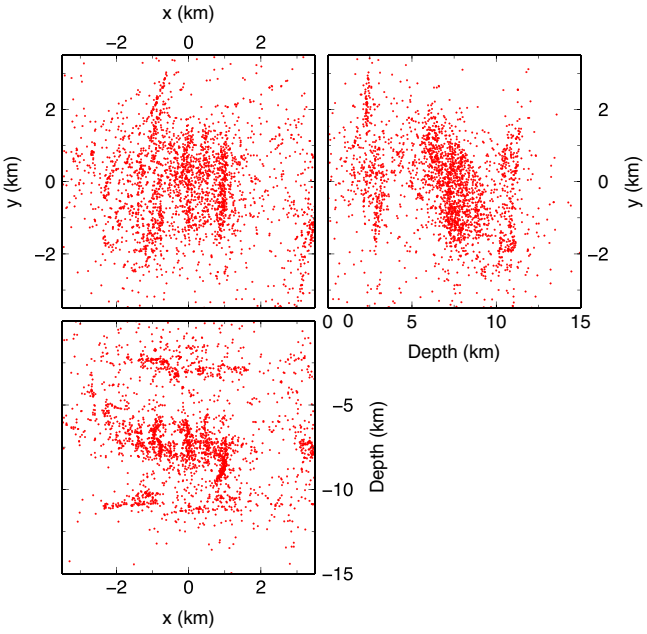

Figure 10. Seismicity in the region indicated in Figure 7, which has been rotated 30° counterclockwise with respect to north to align parallel seismicity streaks along the vertical axis. Plot origin is (–155.445°, 19.485°).

[41] Another prominent and robust feature of our relocated seismicity shown in Figure 9 is the parallel lines of seismicity centered on approximately (–155.445°, 19.485°). An expanded view of these events is shown in Figure 10. The parallel linear features, which strike at 30° and dip about 41° to the southwest, were also identified in the relocation work by *Got and Okubo* [2003] and were interpreted as a zone of strike-slip faults. Our results show about five of these features; their strike is approximately parallel to the topographic contour lines in this area. We also observe horizontal features above and below the vertical faults (Figure 10), which were not observed in the work by *Got and Okubo* [2003]. We note that Figure 9a shows that the horizontal features are in different similar-event clusters from the vertical streaks; the lower and upper horizontal features are also in separate similar-event clusters, even though they appear with a similar purple color in Figure 9a. The lower horizontal feature appears to be a northward extension of the décollement surface visible in Figure 9a.

5.3. Kilauea's South Flank

[42] Relocation results for Kilauea's south flank are shown in Figure 11 and reveal an enhanced sharpening of seismicity into linear features. We find many streaks that appear to align with the direction of geodetic slip vectors (Figure 11b) [*Rubin et al.*, 1999; *Wolfe et al.*, 2007].

[43] The depth and geometry of seismicity in this region are of considerable interest because it may delineate Kilauea's inferred décollement and also because triggered seismicity is useful for constraining the depth of slow-slip events [*Segall et al.*, 2006a; 2006b; *Wolfe et al.*, 2007; *Syracuse et al.*, 2010]. Figure 11a shows a diffuse zone of south flank seismicity in the original catalog, with a lower depth envelope of around 10–12 km. In the relocations (Figure 11b), the events collapse much more sharply in depth, with the seismicity having a peak modal depth of about 6.1 km (below mean station elevation). However, applying the correction to align with the 3-D locations (section 4.4), the peak modal depth shifts to about 7.6 km (below mean sea level; not shown on Figure 11). Therefore, our results show a pronounced sharpening of seismicity along structures consistent with the décollement, but the absolute depth of this surface in our catalog is likely reliable to only about ±1–2 km. However, even in joint hypocenter and 3-D velocity model inversion [*Lin et al.*, 2012], there is a trade-off between depth, average velocity, and origin time, so the absolute depths in the 3-D locations are not necessarily better than in the 1-D locations. We note that double-difference relocation with a 3-D velocity model by *Got et al.* [2008] obtained a depth of about 8 km (below mean sea level) in this region, consistent with the value of 7.6 km obtained here.

[44] We note that the 3-D velocity model tends to reduce the depth of the décollement in the region between Mauna Loa and Kilauea (section 5.2), but tends to increase the depth in Kilauea's south flank. This is likely because some steps were taken to reduce the effect of topography in the 3-D locations [*Lin et al.*, 2012], whereas topography was neglected in our 1-D locations. In the 3-D locations [*Lin et al.*, 2012], two steps were taken to reduce the effects of topography. First, a layer of unmodeled nodes was included a short distance above the highest-elevation station, which relieves topography and avoids air quakes [*Dawson et al.*, 1992]. Second, ray tracing was performed with respect to station elevations. Therefore, topography is not directly but partially accounted for during the 3-D relocation [*Lin et al.*, 2012]. Accurately resolving absolute depths will require both 3-D velocity structure and topography to be accounted for [*Monteiller et al.*, 2005; *Got et al.*, 2008].

5.4. Kealakekua Fault Zone

[45] Figure 12 shows seismicity in the Kealakekua region on the west flank of Mauna Loa (see Figure 7), comparing the relocation results of *Wolfe et al.* [2004] with our HVO1DXC relocated seismicity. *Wolfe et al.* [2004] relocated 3623 events from 1988 to 1998 using cross correlation and the HypoDD algorithm [*Waldhauser and Ellsworth*, 2000]. Of the 3623 relocated events, 1758 overlapped with our studied time period and were relocated in the HVO1DXC catalog. Figure 12a shows all the events relocated by *Wolfe et al.* [2004] within the region indicated on Figure 7 (compare with Figure 19 in the study by *Wolfe et al.* [2004]). Figure 12b shows all events from the HVO1DXC catalog within this region, with more than double the number of events relocated by *Wolfe et al.* [2004]. In Figures 12c and 12d, we show relocations common to both catalogs.

[46] We find excellent agreement between the two catalogs, which provides validation of our relocation method. Similar to *Wolfe et al.* [2004], we find that the relocated seismicity is localized in depth and is consistent with the Kealakekua fault zone reflecting an inland-dipping low-angle detachment.

5.5. Mantle Fault Zones

[47] *Wolfe et al*. [2003, 2004] also relocated 7034 earthquakes with initial depths ≥13 km occurring between 1988

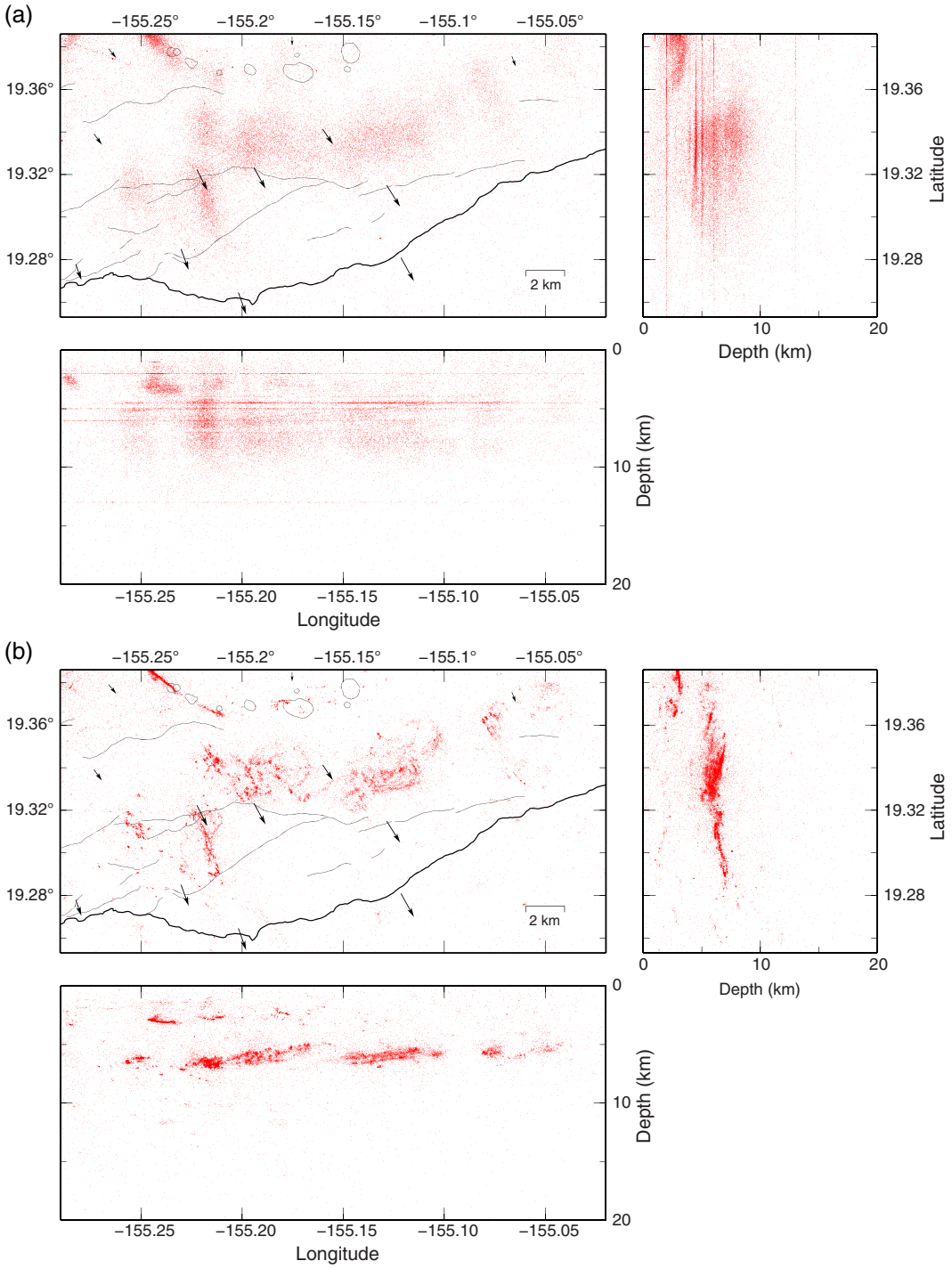

Figure 11. Seismicity in the Kilauea south flank region indicated in Figure 7 for (a) original CUSP catalog locations and (b) relocated catalog, HVO1DXC. Arrows indicate long-term average GPS directions for décollement creep [*Wolfe et al.*, 2007].

and 1998, which we compare to our relocation results in Figure 13. Figure 13 is windowed to approximately correspond to Figure 2 of *Wolfe et al.* [2003]. Our relocation results are consistent with those obtained by *Wolfe et al.* [2003, 2004], particularly when comparing events common to both catalogs (Figures 13c and 13d).

[48] Figure 13b shows a horizontally aligned planar feature at around 30 km depth, consistent with the interpretation of a mantle fault zone [*Wolfe et al.*, 2003, 2004]. The greater number of events in HVO1DXC (Figure 13b) results in a slightly more diffuse depth distribution near 30 km than obtained by *Wolfe et al.* [2003]. It is possible that some of this added scatter in depth arises from our difficulty in constraining absolute depth for deep seismicity with the seismic network geometry and a 1-D velocity model, as discussed in section 5.2.

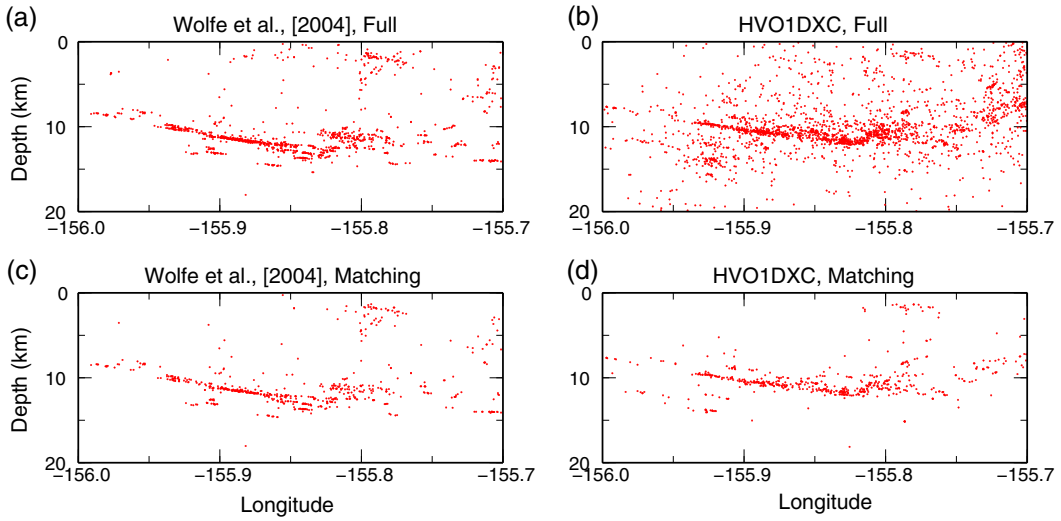

Figure 12. Seismicity in the Kealakekua region indicated on Figure 7. We compare the HVO1DXC relocation results with those of *Wolfe et al.* [2004] in the same region. (a) All events relocated by *Wolfe et al.* [2004] in this region (1077 events), (b) all HVO1DXC events (this study) in this region (2224 events), (c) subset of events from the *Wolfe et al.* [2004] catalog that are also included in the HVO1DXC catalog (592 events), and (d) subset of events in the HVO1DXC catalog that are also included in the *Wolfe et al.* [2004] catalog (570 events).

6. Discussion and Conclusions

[49] We analyzed waveform data from over 130,000 seismic events from January 1992 to March 2009 recorded by the HVO permanent seismic network, computing precise relative relocations for 101,390 events. In general, the relocation procedure results in a dramatic sharpening of seismicity features associated with Hawaii's active volcanic and tectonic processes. Highlights from our relocation results include enhanced pictures of Mauna Loa's south flank seismicity and numerous streaks on Kilauea's south

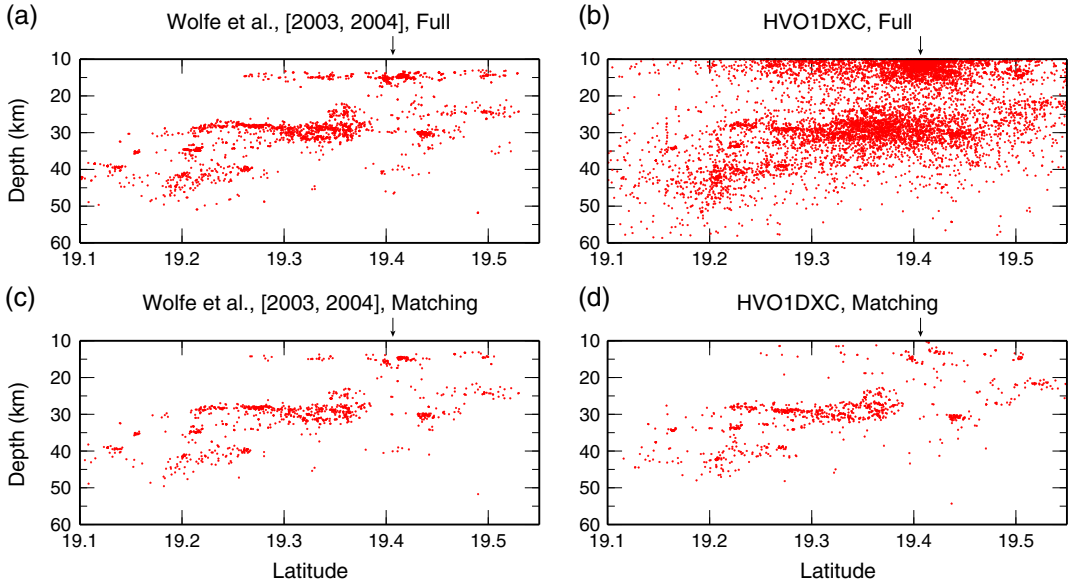

Figure 13. Deeper seismicity beneath Kilauea (10–60 km depth, see Figure 7), where relocations collapse to an inferred deep mantle fault zone [*Wolfe et al.*, 2003, 2004]. An arrow marks the latitude of Halemaumau. (a) All events relocated by *Wolfe et al.* [2003, 2004] in this region (2606 events), (b) all HVO1DXC events (this study) in this region (9406 events), (c) subset of events from the *Wolfe et al.* [2003, 2004] catalog that are also included in the HVO1DXC catalog (1193 events), and (d) subset of events in the HVO1DXC catalog that are also included in the *Wolfe et al.* [2003, 2004] catalog (1118 events).

flank detachment aligned parallel to geodetic slip. Hawaii's value as a natural laboratory for studying seismicity and deformation associated with volcanic and tectonic processes has long been recognized. We anticipate that our catalog will be useful to a variety of researchers studying all aspects of seismicity and deformation on Hawaii Island.

[50] An ultimate goal of earthquake relocation studies is to integrate the algorithms into operational near-real-time network processing, so that new events can be located with the same accuracy as the complete relocated catalog [e.g., *Got et al.*, 2002; *Shearer et al.*, 2005; *Lin et al.*, 2007; *Waldhauser*, 2009]. This may have particularly useful application in volcano monitoring and hazard mitigation; it would be useful to track spatiotemporal evolution of seismicity to high precision in near real time. As discussed by *Shearer et al.* [2005], the difficulty with using the method in real time is that the earthquake location solutions are dependent on all linking events. In principle, a newly added event would affect the locations of all previous nearby seismicity, and the whole catalog would have to be recomputed whenever a new event is added. A reasonable compromise is to redo the entire catalog at fixed time intervals, e.g., once per year. Between these time intervals, new events can be relocated while holding all prior events fixed [*Got et al.*, 2002; *Waldhauser*, 2009].

[51] Our HVO1DXC catalog represents a first attempt to perform relocation of seismicity for the whole island of Hawaii in a systematic way. We have built extensively on previous relocation studies that have focused on smaller subregions of the island, although often considering tens of thousands of events [e.g., *Got et al.*, 1994; *Gillard et al.*, 1996; *Battaglia et al.*, 2003; *Got and Okubo*, 2003; *Wolfe et al.*, 2004; *Syracuse et al.*, 2010]. Our results are generally consistent with those of previous relocation studies, but our catalog includes a much greater number of events, better illuminating seismicity patterns. In addition to updating the catalog in future as more data become available, other possible improvements include (1) extending the catalog back in time by considering digital waveform data available from the mid-1980s onward; (2) incorporating additional seismic stations from temporary networks, e.g., the broadband network around Kilauea [*Dawson et al.*, 1998]; (3) optimizing waveform cross correlation and relocation parameters for LP events [e.g., *Got et al.*, 2002; *Battaglia et al.*, 2003; *Okubo and Wolfe*, 2008]; (4) improving both absolute and relative location accuracy of the reference catalog using, e.g., the source-specific station term (SSST) method and a 3-D velocity model [*Lin et al.*, 2012]; and (5) extension of these algorithms to near-real-time processing [*Got et al.*, 2002; *Waldhauser*, 2009].

[52] **Acknowledgments.** We thank the staff of the USGS Hawaiian Volcano Observatory for maintaining the seismic network and for many valuable discussions, and James Foster for providing the geodetic slip vectors. We made plots using the GMT software [*Wessel and Smith*, 1991]. We thank Jean-Luc Got, David Oppenheimer, and an anonymous reviewer for their useful comments. This work was funded by NSF awards EAR-1045042 and EAR-1246935, and RSM gratefully acknowledges additional support from the Cecil H. and Ida M. Green Foundation at the Institute of Geophysics and Planetary Physics, Scripps Institution of Oceanography. The HVO1DXC catalog is available for download in the supporting information. Updates to the catalog will be available at http://igppweb.ucsd.edu/~rmatoza.

References

Aki, K., and R. Koyanagi (1981), Deep volcanic tremor and magma ascent mechanism under Kilauea, Hawaii, *J. Geophys. Res.*, *86*(B8), 7,095–7,109.

Almendros, J., B. Chouet, and P. Dawson (2001), Spatial extent of a hydrothermal system at Kilauea Volcano, Hawaii, determined from array analyses of shallow long-period seismicity 2. Results, *J. Geophys. Res.*, *106*(B8), 13,581–13,597.

Battaglia, J., J.-L. Got, and P. Okubo (2003), Location of long-period events below Kilauea Volcano using seismic amplitudes and accurate relative relocation, *J. Geophys. Res.*, *108*(B12), 2553, doi:10.1029/2003JB002517.

Brooks, B. A., J. H. Foster, M. Bevis, L. N. Frazer, C. J. Wolfe, and M. Behn (2006), Periodic slow earthquakes on the flank of Kilauea volcano, Hawaii, *Earth Planet. Sci. Lett.*, *246*, 207–216.

Cervelli, P., P. Segall, K. Johnson, M. Lisowski, and A. Miklius (2002), Sudden aseismic fault slip on the south flank of Kilauea volcano, *Nature*, *415*, 1014–1018.

Chouet, B., and P. Dawson (2011), Shallow conduit system at Kilauea Volcano, Hawaii, revealed by seismic signals associated with degassing bursts, *J. Geophys. Res.*, *116*, B12317, doi:10.1029/2011JB008677.

Chouet, B. A. (1996a), New methods and future trends in seismological volcano monitoring, in *Monitoring and Mitigation of Volcano Hazards*, edited by R. Scarpa and R. I. Tilling, 23–97, Springer-Verlag, New York.

Chouet, B. A. (1996b), Long-period volcano seismicity: Its source and use in eruption forecasting, *Nature*, *380*, 309–316.

Chouet, B. A., P. B. Dawson, M. R. James, and S. J. Lane (2010), Seismic source mechanism of degassing bursts at Kilauea volcano, Hawaii: Results from waveform inversion in the 10–50 s band, *J. Geophys. Res.*, *115*, B09311.

Dawson, P. B., B. Chouet, J. C. Lahr, and R. A. Page (1992), Spatial relationship between LP earthquakes and a shallow three-dimensional velocity anomaly beneath Redoubt Volcano, Alaska, *Eos, Trans. AGU*, *73*, 343.

Dawson, P. B., C. Dietel, B. A. Chouet, K. Honma, T. Ohminato, and P. Okubo (1998), A digitally telemetered broadband seismic network at Kilauea Volcano, Hawaii, *U.S. Geological Survey Open-File Report, 98–108.*

Dawson, P. B., M. C. Benitez, B. A. Chouet, D. Wilson, and P. G. Okubo (2010), Monitoring very-long-period seismicity at Kilauea Volcano, Hawaii, *Geophys. Res. Lett.*, *37*, L18306, doi:10.1029/2010GL044418.

Douglas, A. (1967), Joint epicentre determination, *Nature*, *215*, 47–48.

Eaton, J. P. (1962), Crustal structure and volcanism in Hawaii, *Geophys. Monogr. Ser.*, *6*, 13–29.

Eaton, J. P., and K. J. Murata (1960), How volcanoes grow, *Science*, *132*(3432), 925–938.

Ferrazzini, V., K. Aki, and B. Chouet (1991), Characteristics of seismic waves composing Hawaiian volcanic tremor and gas-piston events observed by a near-source array, *J. Geophys. Res.*, *96*(B4), 6199–6209.

Fréchet, J (1985), Sismogenèse et doublets sismiques, Thèse d'Etat, Univ. Sci. Technol. Médic., Grenoble.

Fremont, M.-J., and S. D. Malone (1987), High precision relative locations of earthquakes at Mount St. Helens, Washington, *J. Geophys. Res.*, *2*(B10), 10,223–10,236.

Frohlich, C. (1979), An efficient method for joint hypocenter determination for large groups of earthquakes, *Comput. Geosci.*, *5*, 387–389.

Gillard, D., A. M. Rubin, and P. Okubo (1996), Highly concentrated seismicity caused by deformation of Kilauea's deep magma system, *Nature*, *384*, 343–346.

Got, J.-L., and P. Okubo (2003), New insights into Kilauea's volcano dynamics brought by large-scale relative relocation of microearthquakes, *J. Geophys. Res.*, *108*(B7), 2337, doi:10.1029/2002JB002060.

Got, J.-L., J. Frechet, and F. W. Klein (1994), Deep fault plane geometry inferred from multiplet relative relocation beneath the south flank of Kilauea, *J. Geophys. Res.*, *99*(B8), 15,375–15,386.

Got, J.-L., P. Okubo, R. Machenbaum, and W. Tanigawa (2002), A real-time procedure for progressive multiplet relative relocation at the Hawaiian Volcano Observatory, *Bull. Seismol. Soc. Am.*, *92*(5), 2019–2026.

Got, J.-L., V. Monteiller, J. Monteux, R. Hassani, and P. Okubo (2008), Deformation and rupture of the oceanic crust may control growth of Hawaiian volcanoes, *Nature*, *451*, 453–456.

Hansen, S., C. Thurber, M. Mandernach, F. Haslinger, and C. Doran (2004), Seismic velocity and attenuation structure of the East Rift Zone and South Flank of Kilauea Volcano, Hawaii, *Bull. Seismol. Soc. Am.*, *94*, 1430–1440.

Hauksson, E., and P. Shearer (2005), Southern California hypocenter relocation with waveform cross-correlation, part 1: Results using the double-difference method, *Bull. Seismol. Soc. Am.*, *95*(3), 896–903.

Hauksson, E., W. Yang, and P. Shearer (2012), Waveform relocated earthquake catalog for southern California (1981 to June 2011), *Bull. Seismol. Soc. Am.*, *102*(5), 2239–2244.

Jaggar, T. A. (1920), Seismometric investigations of the Hawaiian lava column, *Bull. Seism. Soc. Am.*, *6*(4), 204.

Kauahikaua, J., and M. Poland (2012), One hundred years of volcano monitoring in Hawaii, *EOS Trans. AGU*, *93*(3), 29–31.

Klein, F. W. (1981), A linear gradient crustal model for south Hawaii, *Bull. Seismol. Soc. Am.*, *71*(5), 1503–1510.

Klein, F. W., and R. Y. Koyanagi (1980), Hawaiian Volcano Observatory seismic network history, 1950–1979, *U.S. Geological Survey Open-File Report, 80–302.*

Klein, F. W., R. Y. Koyanagi, J. S. Nakata, and W. R. Tanigawa (1987), The seismicity of Kilauea's magma system, in *Volcanism in Hawaii*, edited by R. W. Decker, T. L. Wright, and P. H. Stauffer, U.S. Geological Survey, Denver, CO, chap. 43, pp. 1019–1185. USGS Prof. Paper 1350(2).

Klein, F. W., A. D. Frankel, C. S. Mueller, R. L. Wesson, and P. G. Okubo (2001), Seismic hazard in Hawaii: High rate of large earthquakes and probabilistic ground-motion maps, *Bull. Seismol. Soc. Am.*, *91*(3), 479–498.

Koyanagi, R. Y., B. Chouet, and K. Aki (1987), Origin of volcanic tremor in Hawaii: Part i. Data from the Hawaiian Volcano Observatory 1969–1985, in *Volcanism in Hawaii*, edited by R. W. Decker, T. L. Wright, and P. H. Stauffer, U.S. Geological Survey, Denver, CO, chap. 43, pp. 1221–1257. USGS Prof. Paper 1350(2).

Kumagai, H., B. A. Chouet, and P. B. Dawson (2005), Source process of a long-period event at Kilauea Volcano, Hawaii, *Geophys. J. Int.*, *161*, 243–254.

Lin, G., and P. Shearer (2005), Tests of relative earthquake location techniques using synthetic data, *J. Geophys. Res.*, *110*, B04304, doi:10.1029/2004JB003380.

Lin, G., P. M. Shearer, and E. Hauksson (2007), Applying a three-dimensional velocity model, waveform cross correlation, and cluster analysis to locate southern California seismicity from 1981 to 2005, *J. Geophys. Res.*, *112*, B12309, doi:10.1029/2007JB004986.

Lin, G., P. M. Shearer, P. G. Okubo, C. J. Wolfe, and F. Amelung (2012), Three-dimensional velocity structure of Kilauea and Mauna Loa Volcanoes from local seismic tomography, *paper presented at AGU Chapman Conference: Hawaiian Volcanoes: From Source to Surface*, Waikoloa, Hawaii.

McGovern, P. J. (2007), Flexural stresses beneath Hawaii: Implications for the October 15, 2006, earthquakes and magma ascent, *Geophys. Res. Lett.*, *34*, L23305, doi:10.1029/2007GL031305.

Monteiller, V., J.-L. Got, J. Virieux, and P. Okubo (2005), An efficient algorithm for double-difference tomography and location in heterogeneous media, with an application to the Kilauea volcano, *J. Geophys. Res.*, *110*, B12306, doi:10.1029/2004JB003466.

Montgomery-Brown, E. K., P. Segall, and A. Miklius (2009), Kilauea slow slip events: Identification, source inversions, and relation to seismicity, *J. Geophys. Res.*, *114*, B00A03, doi:10.1029/2008JB006074.

Moore, J. G., W. R. Normack, and R. T. Holcomb (1994), Giant Hawaiian underwater landslides, *Science*, *264*, 46–47.

Nadeau, R. M., W. Foxall, and T. V. McEvilly (1995), Clustering and periodic recurrence of microearthquakes on the San Andreas Fault at Parkfield, California, *Science*, *267*, 503–507.

Nakata, J. (2007), Hawaiian Volcano Observatory seismic data, January to December 2006, *U.S. Geological Survey Open-File Report, 2007–1073.*

Nakata, J. S., and P. G. Okubo, (2010), Hawaiian Volcano Observatory seismic data, January to March 2009, *U.S. Geological Survey Open-File Report, 2010–1079.*

Neal, C. A., and J. P. Lockwood (2003), Geologic map of the summit region of Kilauea Volcano, Hawaii, *U.S. Geological Survey Geological Investigations Series, I-2759.*

Ohminato, T., B. A. Chouet, P. B. Dawson, and S. Kedar (1998), Waveform inversion of very-long-period impulsive signals associated with magmatic injection beneath Kilauea Volcano, Hawaii, *J. Geophys. Res.*, *103*, 23,839–23,862.

Okubo, P. G., and C. J. Wolfe (2008), Swarms of similar long-period earthquakes in the mantle beneath Mauna Loa Volcano, *J. Volcanol. Geotherm. Res.*, *178*, 787–794.

Owen, S., P. Segall, J. Freymueller, A. Miklius, R. Denlinger, T. Arnadottir, M. Sako, and R. Burgmann (1995), Rapid deformation of the south flank of Kilauea Volcano, Hawaii, *Science*, *267*, 1328–1332.

Owen, S., P. Segall, M. Lisowski, A. Miklius, R. Denlinger, and M. Sako (2000), Rapid deformation of Kilauea Volcano: Global positioning system measurements between 1990 and 1996, *J. Geophys. Res.*, *105*(B8), 18,983–18,998.

Patrick, M. R., T. Orr, D. Wilson, D. Dow, and R. Freeman (2011), Cyclic spattering, seismic tremor, and surface fluctuation within a perched lava channel, Kilauea Volcano, *Bull. Volcanol.*, *73*, 639–653.

Pritchard, M. E., A. M. Rubin, and C. J. Wolfe (2007), Do flexural stresses explain the mantle fault zone beneath Kilauea volcano? *Geophys. J. Int.*, *168*, 419–430.

Richards-Dinger, K. B., and P. M. Shearer (2000), Earthquake locations in southern California obtained using source-specific station terms, *J. Geophys. Res.*, *105*(B5), 10,939–10,960

Rubin, A. M., D. Gillard, and J.-L. Got (1999), Streaks of microearthquakes along creeping faults, *Nature*, *400*, 635–641.

Ryan, M. P. (1988), The mechanics and three-dimensional internal structure of active magmatic systems: Kilauea Volcano, Hawaii, *J. Geophys. Res.*, *93*(B5), 4213–4248

Saccorotti, G., B. Chouet, and P. Dawson (2001), Wavefield properties of a shallow long-period event and tremor at Kilauea Volcano, Hawaii, *J. Volcanol. Geotherm. Res.*, *109*, 163–189.

Segall, P., E. K. Desmarais, D. Shelly, A. Miklius, and P. Cervelli (2006a), Corrigendum to "Earthquakes triggered by silent slip events on Kilauea volcano, Hawaii", *Nature*, *444*, 235.

Segall, P., E. K. Desmarais, D. Shelly, A. Miklius, and P. Cervelli (2006b), Earthquakes triggered by silent slip events on Kilauea volcano, Hawaii, *Nature*, *442*, 71–74.

Shaw, H. R., and B. Chouet (1989), Singularity spectrum of intermittent seismic tremor at Kilauea Volcano, Hawaii, *Geophys. Res. Lett.*, *16*(2), 195–198.

Shearer, P., E. Hauksson, and G. Lin (2005), Southern California hypocenter relocation with waveform cross-correlation, part 2: Results using source-specific station terms and cluster analysis, *Bull. Seismol. Soc. Am.*, *95*(3), 904–915.

Shearer, P. M. (1997), Improving local earthquake locations using the L1 norm and waveform cross correlation: Application to the Whittier Narrows, California, aftershock sequence, *J. Geophys. Res.*, *102*(B4), 8,269–8,283.

Swanson, D. A., W. A. Duffield, and R. S. Fiske (1976), Displacement of the south flank of Kilauea Volcano: The result of forceful intrusion of magma into the rift zones, *U.S. Geological Survey Professional Paper*, *963*, 39.

Swanson, D. A., W. A. Duffield, D. B. Jackson, and D. W. Peterson (1979), Chronological narrative of the 1969–1971 Mauna Ulu eruption of Kilauea Volcano, Hawaii, *U.S. Geological Survey Professional Paper, 1056.*

Syracuse, E. M., C. H. Thurber, C. J. Wolfe, P. G. Okubo, J. H. Foster, and B. A. Brooks (2010), High-resolution locations of triggered earthquakes and tomographic imaging of Kilauea Volcano's south flank, *J. Geophys. Res.*, *115*, B10310, doi:10.1029/2010JB007554.

Tilling, R. I., and J. J. Dvorak (1993), Anatomy of a basaltic volcano, *Nature*, *363*, 125–133.

Waldhauser, F. (2009), Near-real-time double-difference event location using long-term seismic archives, with application to Northern California, *Bull. Seismol. Soc. Am.*, *99*(5), 2736–2748.

Waldhauser, F., and W. L. Ellsworth (2000), A double-difference earthquake location algorithm: Method and application to the Northern Hayward Fault, California, *Bull. Seismol. Soc. Am.*, *90*(6), 1353–1368.

Waldhauser, F., W. L. Ellsworth, and A. Cole (1999), Slip-parallel seismic lineations on the northern Hayward Fault, California, *Geophys. Res. Lett.*, *26*(23), 3525–3528.

Walter, T. R., and F. Amelung (2004), Influence of volcanic activity at Mauna Loa, Hawaii, on earthquake occurrence in the Kaoiki Seismic Zone, *Geophys. Res. Lett.*, *31*, L07622, doi:10.1029/2003GL019131.

Ward, S. N. (2002), Slip-sliding away, *Nature*, *415*, 973–974.

Wessel, P., and W. H. F. Smith (1991), Free software helps map and display data, *EOS Trans. AGU*, *72*(41), 441.

Wolfe, C. J., P. G. Okubo, and P. M. Shearer (2003), Mantle fault zone beneath Kilauea Volcano, Hawaii, *Science*, *300*, 478–480.

Wolfe, C. J., P. G. Okubo, G. Ekstrom, M. Nettles, and P. M. Shearer (2004), Characteristics of deep ($\geq$13 km) Hawaiian earthquakes and Hawaiian earthquakes west of 155.55°W, *Geochem. Geophys. Geosyst.*, *5*, Q04006, doi:10.1029/2003GC000618.

Wolfe, C. J., B. A. Brooks, J. H. Foster, and P. G. Okubo (2007), Microearthquake streaks and seismicity triggered by slow earthquakes on the mobile south flank of Kilauea Volcano, Hawaii, *Geophys. Res. Lett.*, *34*, L23306, doi:10.1029/2007GL031625.

Wright, T. L., and F. W. Klein (2006), Deep magma transport at Kilauea volcano, Hawaii, *Lithos*, *87*, 50–79.

Yamada, T., P. G. Okubo, and C. J. Wolfe (2010), Kiholo Bay, Hawai'i, earthquake sequence of 2006: Relationship of the main shock slip with locations and source parameters of aftershocks, *J. Geophys. Res.*, *115*, B08304, doi:10.1029/2009JB006657.